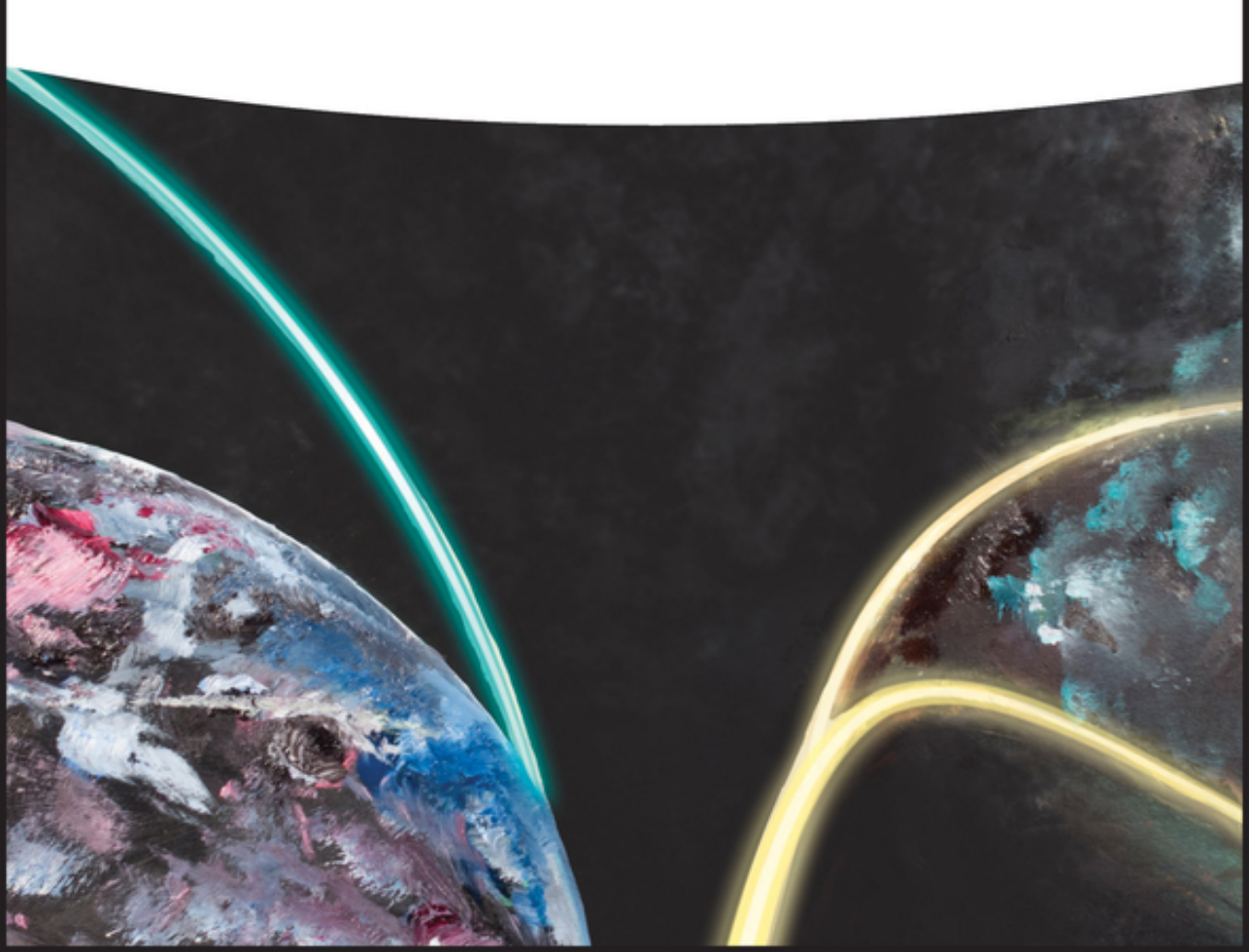
Edited by Ralf Zimmermann and Luke Hanley

Photoionization and Photo-Induced Processes in Mass Spectrometry

Fundamentals and Applications



Photoionization and Photo-Induced Processes in Mass Spectrometry	

Photoionization and Photo-Induced Processes in Mass Spectrometry

Fundamentals and Applications

Edited by

Ralf Zimmermann Luke Hanley



Editors

Ralf Zimmermann

Helmholtz Zentrum München Institut für Ökologische Chemie Ingolstädter Landstr. 1 85764 Oberschleißheim Germany

Luke Hanley

University of Illinois Department of Chemistry United States

Cover Images: Courtesy of Jonathan Aldrich, The University of Illinois at Chicago All books published by Wiley-VCH are carefully produced. Nevertheless, authors, editors, and publisher do not warrant the information contained in these books, including this book, to be free of errors. Readers are advised to keep in mind that statements, data, illustrations, procedural details or other items may inadvertently be inaccurate.

Library of Congress Card No.: applied for

British Library Cataloguing-in-Publication Data

A catalogue record for this book is available from the British Library.

Bibliographic information published by the Deutsche Nationalbibliothek

The Deutsche Nationalbibliothek lists this publication in the Deutsche Nationalbibliografie; detailed bibliographic data are available on the Internet at http://dnb.d-nb.de>.

© 2021 WILEY-VCH GmbH, Boschstr. 12, 69469 Weinheim, Germany

All rights reserved (including those of translation into other languages). No part of this book may be reproduced in any form – by photoprinting, microfilm, or any other means – nor transmitted or translated into a machine language without written permission from the publishers. Registered names, trademarks, etc. used in this book, even when not specifically marked as such, are not to be considered unprotected by law.

Print ISBN: 978-3-527-33510-7 ePDF ISBN: 978-3-527-68223-2 ePub ISBN: 978-3-527-68222-5 oBook ISBN: 978-3-527-68220-1

Cover Design: Wiley
Typesetting SPi Global, Chennai, India
Printing and Binding

Printed on acid-free paper

10 9 8 7 6 5 4 3 2 1

Contents

Preface xi

1	Fundamentals and Mechanisms of Vacuum Photoionization $\ 1$
	Johannes Passig, Ralf Zimmermann, and Thomas Fennel
1.1	Preface 1
1.2	Light 2
1.3	Photoabsorption 5
1.3.1	Transitions in First Order Perturbation Theory 5
1.3.2	Perturbation Theory 6
1.3.3	Absorption 7
1.3.4	Dipole Approximation 9
1.3.5	Selection Rules 11
1.3.6	Electronic Line Width and Lifetime 11
1.3.7	Electronic Transitions of Molecules 13
1.3.8	Single-photon Ionization (SPI) 15
	References 20
2	Fundamentals and Mechanisms of Resonance-Enhanced
	Multiphoton Ionization (REMPI) in Vacuum and its Application
	Multiphoton Ionization (REMPI) in Vacuum and its Application in Molecular Spectroscopy 23
2.1	in Molecular Spectroscopy 23
2.1 2.2	in Molecular Spectroscopy 23 Ulrich Boesl and Ralf Zimmermann
	in Molecular Spectroscopy 23 Ulrich Boesl and Ralf Zimmermann Introductory Remarks 23
2.2	in Molecular Spectroscopy 23 Ulrich Boesl and Ralf Zimmermann Introductory Remarks 23 Beginnings of REMPI 25
2.2	in Molecular Spectroscopy 23 Ulrich Boesl and Ralf Zimmermann Introductory Remarks 23 Beginnings of REMPI 25 Principle of REMPI: Rate Equations and Quantification of Detection
2.2 2.3	in Molecular Spectroscopy 23 Ulrich Boesl and Ralf Zimmermann Introductory Remarks 23 Beginnings of REMPI 25 Principle of REMPI: Rate Equations and Quantification of Detection Efficiency 29
2.2 2.3 2.3.1	in Molecular Spectroscopy 23 Ulrich Boesl and Ralf Zimmermann Introductory Remarks 23 Beginnings of REMPI 25 Principle of REMPI: Rate Equations and Quantification of Detection Efficiency 29 Rate Equations 29
2.2 2.3 2.3.1 2.3.2	in Molecular Spectroscopy 23 Ulrich Boesl and Ralf Zimmermann Introductory Remarks 23 Beginnings of REMPI 25 Principle of REMPI: Rate Equations and Quantification of Detection Efficiency 29 Rate Equations 29 Quantification of the REMPI Detection Efficiency 31
2.2 2.3 2.3.1 2.3.2	in Molecular Spectroscopy 23 Ulrich Boesl and Ralf Zimmermann Introductory Remarks 23 Beginnings of REMPI 25 Principle of REMPI: Rate Equations and Quantification of Detection Efficiency 29 Rate Equations 29 Quantification of the REMPI Detection Efficiency 31 Special Situations and Problems in REMPI Processes and
2.2 2.3 2.3.1 2.3.2 2.3.3	in Molecular Spectroscopy 23 Ulrich Boesl and Ralf Zimmermann Introductory Remarks 23 Beginnings of REMPI 25 Principle of REMPI: Rate Equations and Quantification of Detection Efficiency 29 Rate Equations 29 Quantification of the REMPI Detection Efficiency 31 Special Situations and Problems in REMPI Processes and Countermeasures 33 Situation (A): Too energetic ionization threshold 34 Situation (B): Too energetic intermediate state 35
2.2 2.3 2.3.1 2.3.2 2.3.3 2.3.3.1	in Molecular Spectroscopy 23 Ulrich Boesl and Ralf Zimmermann Introductory Remarks 23 Beginnings of REMPI 25 Principle of REMPI: Rate Equations and Quantification of Detection Efficiency 29 Rate Equations 29 Quantification of the REMPI Detection Efficiency 31 Special Situations and Problems in REMPI Processes and Countermeasures 33 Situation (A): Too energetic ionization threshold 34
2.2 2.3 2.3.1 2.3.2 2.3.3 2.3.3.1 2.3.3.2	in Molecular Spectroscopy 23 Ulrich Boesl and Ralf Zimmermann Introductory Remarks 23 Beginnings of REMPI 25 Principle of REMPI: Rate Equations and Quantification of Detection Efficiency 29 Rate Equations 29 Quantification of the REMPI Detection Efficiency 31 Special Situations and Problems in REMPI Processes and Countermeasures 33 Situation (A): Too energetic ionization threshold 34 Situation (B): Too energetic intermediate state 35
2.2 2.3 2.3.1 2.3.2 2.3.3 2.3.3.1 2.3.3.2 2.3.3.3	in Molecular Spectroscopy 23 Ulrich Boesl and Ralf Zimmermann Introductory Remarks 23 Beginnings of REMPI 25 Principle of REMPI: Rate Equations and Quantification of Detection Efficiency 29 Rate Equations 29 Quantification of the REMPI Detection Efficiency 31 Special Situations and Problems in REMPI Processes and Countermeasures 33 Situation (A): Too energetic ionization threshold 34 Situation (B): Too energetic intermediate state 35 Situation (C): Too small FC-factors 36

vi	Contents	
	2.5	Application of REMPI for Optical Spectroscopy 45
	2.5.1	Effusive Gas Beam Molecules at Room or Elevated Temperature: REMPI Spectra with Medium Optical Selectivity 45
	2.5.2	Supersonic Gas Beams for Cold Molecules: REMPI Spectra with High Optical Selectivity for Discrimination of Structural Isomers and Spectroscopic Studies on the Transition State 48
	2.5.2.1	REMPI Spectroscopy of Jet-Cooled Biphenylene 50
	2.5.2.2	REMPI Spectroscopy of Jet-Cooled Dibenzo-p-dioxin and Its
		Derivatives as well as of [2,2]-Paracyclophane 61
	2.5.3	Supersonic Gas Beams for Cold Molecules: REMPI Spectra with High Optical Selectivity for Discrimination of Isotopomers 67
	2.5.4	Chiral Molecules: Discrimination of Enantiomers by Enantioselective REMPI Spectroscopy 69
	2.5.5	Advanced Photoelectron Spectroscopy Based on REMPI: The PES, TPES, ZEKE, MATI, Anion-PES, and Anion-ZEKE Approaches 72
		References 79
	3	Analytical Application of Single-Photon Ionization Mass
		Spectrometry (SPI-MS) 89
		Thorsten Streibel, Hendryk Czech, and Ralf Zimmermann
	3.1	VUV Light Sources 89
	3.2	Lamp-Based VUV Light Sources 90
	3.3	Laser-Based VUV Light Sources 92
	3.4	Mass Spectrometry with Lamp or Laser-Based VUV Light Sources 94
	3.5	On-line Analysis of Complex Mixtures by Single-Photon Ionization (SPI) Mass Spectrometry 95
	3.6	SPI-MS in Hyphenated Applications 107
	3.7	Ambient Monitoring 117
	3.8	Commercial Solutions 118
		References 119
	4	Analytical Application of Resonance-Enhanced Multiphoton
		Ionization Mass Spectrometry (REMPI-MS) 125
		Thorsten Streibel, Ulrich Boesl, and Ralf Zimmermann
	4.1	Investigation of Model Flames 129
	4.2	Applications to Internal Combustion Engines 130

Monitoring Combustion Process Emissions in an Industrial

Further Applications of REMPI Mass Spectrometry 138

Commercial REMPI-MS Solutions and Applications 150

REMPI-MS in Hyphenated Analytical Systems 142

4.3

4.4

4.5

4.6

Environment 135

References 152

5	Probing Chemistry at Vacuum Ultraviolet Synchrotron Light	
	Sources 159	
	Kevin R. Wilson and Fei Qi	
5.1	Introduction 159	
5.2	Combustion Chemistry 162	
5.2.1	Pyrolysis in Flow Reactor 163	
5.2.2	Jet-Stirred Reactor Oxidation 166	
5.2.3	Premixed Flames 167	
	Low-Pressure Laminar Premixed Flame 167	
5.2.3.2	Atmospheric Pressure Laminar Premixed Flame 171	
5.2.4	Coflow Diffusion Flame 173	
5.2.5	Biomass/Coal Pyrolysis 174	
5.3	Isomer-Resolved Studies of Elementary Chemical Reactions 17	76
5.3.1	Multiplexed Chemical Kinetics Photoionization Mass	
5.5.1	Spectrometer 177	
5.3.2	Shock Tube Kinetics 179	
5.3.3	Pyrolysis Reactors 180	
	Bimolecular Kinetics 181	
	Unimolecular Kinetics 181	
5.3.4	Low-Temperature Elementary Reactions in a Pulsed Laval	
5.5.1	Nozzle 182	
5.4	Summary 186	
5.4.1	Atmospheric Aerosol Chemistry 188	
5.4.1.1	•	
5.4.1.2	÷ '	
J. I.1.2	Spectrometry 195	
5.4.2	Future Outlook 202	
J. I.2	Acknowledgments 203	
	References 203	
	References 200	
6	Resonance Ionization Mass Spectrometry (RIMS):	
•	Fundamentals and Applications Including Secondary Neutral	
	Mass Spectrometry 215	
	Michael Savina and Reto Trappitsch	
6.1	Introduction 215	
6.2	Resonance Ionization Fundamentals 217	
6.2.1	Laser Spectroscopy 217	
6.2.2	Selection Rules 220	
6.2.3	Odd–Even Effect 222	
6.3	Reduction to Practice 224	
6.3.1	Laser Selection 224	
6.3.2	Mass Spectrometer Selection 225	
6.3.3	Laser Overlap 229	
6.4	Applications 230	
6.4.1	Useful Yield and Abundance Sensitivity 231	
J. I. I	Oscial field and ribundance scristivity 251	

viii	Contents	
	612	

6.4.2 6.4.3	Stardust Grains 234 Multielement Analysis 236
6.4.4	Electronic Processes During Vaporization 238
6.5	Resources 240
	References 241
7	Ultrashort Pulse Photoionization for Femtosecond Laser Mass
	Spectrometry 245
	Cornelius L. Pieterse, Jason M. Gross, and Luke Hanley
7.1	Introduction 245
7.2	Mechanisms of Ultrashort Pulse Photoionization 246
7.3	Studies of Amino Acids, Dipeptides, and C_{60} Leading to Advanced SFI Models 249
7.4	Volumetric Intensity Dependence and Multiply Charged Ions 251
7.5	Direct and Gas Chromatography-Coupled Analysis of Explosives 253
7.6	Gas Chromatography-Coupled Analysis of Polyaromatic
	Hydrocarbons, Pesticides, and Fragrances 255
7.7	Laser Secondary Neutral Mass Spectrometry 256
7.8	Conclusions 259
	Acknowledgments 260
	Disclosure Statement 260
	References 261
8	Photoionization at Elevated or Atmospheric Pressure:
8	Photoionization at Elevated or Atmospheric Pressure: Applications of APPI and LPPI 267
8	
8 8.1	Applications of APPI and LPPI 267
	Applications of APPI and LPPI 267 Tiina J. Kauppila and Jack Syage
8.1	Applications of APPI and LPPI 267 Tiina J. Kauppila and Jack Syage Introduction 267
8.1 8.2	Applications of APPI and LPPI 267 Tiina J. Kauppila and Jack Syage Introduction 267 Atmospheric Pressure Photoionization 267
8.1 8.2 8.2.1	Applications of APPI and LPPI 267 Tiina J. Kauppila and Jack Syage Introduction 267 Atmospheric Pressure Photoionization 267 Atmospheric Pressure Photoionization Ion Source 267
8.1 8.2 8.2.1 8.2.2	Applications of APPI and LPPI 267 Tiina J. Kauppila and Jack Syage Introduction 267 Atmospheric Pressure Photoionization 267 Atmospheric Pressure Photoionization Ion Source 267 General Principles of Atmospheric Pressure Photoionization 268
8.1 8.2 8.2.1 8.2.2 8.2.2.1	Applications of APPI and LPPI 267 Tiina J. Kauppila and Jack Syage Introduction 267 Atmospheric Pressure Photoionization 267 Atmospheric Pressure Photoionization Ion Source 267 General Principles of Atmospheric Pressure Photoionization 268 Ionization Mechanism in Positive Ion APPI 268
8.1 8.2 8.2.1 8.2.2 8.2.2.1 8.2.2.2	Applications of APPI and LPPI 267 Tiina J. Kauppila and Jack Syage Introduction 267 Atmospheric Pressure Photoionization 267 Atmospheric Pressure Photoionization Ion Source 267 General Principles of Atmospheric Pressure Photoionization 268 Ionization Mechanism in Positive Ion APPI 268 Effect of the Dopant 270
8.1 8.2 8.2.1 8.2.2 8.2.2.1 8.2.2.2 8.2.2.3	Applications of APPI and LPPI 267 Tiina J. Kauppila and Jack Syage Introduction 267 Atmospheric Pressure Photoionization 267 Atmospheric Pressure Photoionization Ion Source 267 General Principles of Atmospheric Pressure Photoionization 268 Ionization Mechanism in Positive Ion APPI 268 Effect of the Dopant 270 Ionization Mechanism in Negative Ion APPI 271
8.1 8.2 8.2.1 8.2.2 8.2.2.1 8.2.2.2 8.2.2.3 8.2.3	Applications of APPI and LPPI 267 Tiina J. Kauppila and Jack Syage Introduction 267 Atmospheric Pressure Photoionization 267 Atmospheric Pressure Photoionization Ion Source 267 General Principles of Atmospheric Pressure Photoionization 268 Ionization Mechanism in Positive Ion APPI 268 Effect of the Dopant 270 Ionization Mechanism in Negative Ion APPI 271 APPI in Liquid Chromatography Mass Spectrometry 272
8.1 8.2 8.2.1 8.2.2 8.2.2.1 8.2.2.2 8.2.2.3 8.2.3 8.2.4	Applications of APPI and LPPI 267 Tiina J. Kauppila and Jack Syage Introduction 267 Atmospheric Pressure Photoionization 267 Atmospheric Pressure Photoionization Ion Source 267 General Principles of Atmospheric Pressure Photoionization 268 Ionization Mechanism in Positive Ion APPI 268 Effect of the Dopant 270 Ionization Mechanism in Negative Ion APPI 271 APPI in Liquid Chromatography Mass Spectrometry 272 APPI in Gas Chromatography Mass Spectrometry 274
8.1 8.2 8.2.1 8.2.2 8.2.2.1 8.2.2.2 8.2.2.3 8.2.3 8.2.4	Applications of APPI and LPPI 267 Tiina J. Kauppila and Jack Syage Introduction 267 Atmospheric Pressure Photoionization 267 Atmospheric Pressure Photoionization Ion Source 267 General Principles of Atmospheric Pressure Photoionization 268 Ionization Mechanism in Positive Ion APPI 268 Effect of the Dopant 270 Ionization Mechanism in Negative Ion APPI 271 APPI in Liquid Chromatography Mass Spectrometry 272 APPI in Gas Chromatography Mass Spectrometry 274 APPI AS an Interface for Capillary Electrophoresis Mass
8.1 8.2 8.2.1 8.2.2 8.2.2.1 8.2.2.2 8.2.2.3 8.2.3 8.2.4 8.2.5	Applications of APPI and LPPI 267 Tiina J. Kauppila and Jack Syage Introduction 267 Atmospheric Pressure Photoionization 267 Atmospheric Pressure Photoionization Ion Source 267 General Principles of Atmospheric Pressure Photoionization 268 Ionization Mechanism in Positive Ion APPI 268 Effect of the Dopant 270 Ionization Mechanism in Negative Ion APPI 271 APPI in Liquid Chromatography Mass Spectrometry 272 APPI in Gas Chromatography Mass Spectrometry 274 APPI As an Interface for Capillary Electrophoresis Mass Spectrometry 277 APPI in Multimode Ion Sources 278 Ambient Mass Spectrometry Utilizing Photoionization 278
8.1 8.2 8.2.1 8.2.2 8.2.2.1 8.2.2.2 8.2.2.3 8.2.3 8.2.4 8.2.5	Applications of APPI and LPPI 267 Tiina J. Kauppila and Jack Syage Introduction 267 Atmospheric Pressure Photoionization 267 Atmospheric Pressure Photoionization Ion Source 267 General Principles of Atmospheric Pressure Photoionization 268 Ionization Mechanism in Positive Ion APPI 268 Effect of the Dopant 270 Ionization Mechanism in Negative Ion APPI 271 APPI in Liquid Chromatography Mass Spectrometry 272 APPI in Gas Chromatography Mass Spectrometry 274 APPI As an Interface for Capillary Electrophoresis Mass Spectrometry 277 APPI in Multimode Ion Sources 278 Ambient Mass Spectrometry Utilizing Photoionization 278 Low-Pressure Photoionization (LPPI) 279
8.1 8.2 8.2.1 8.2.2 8.2.2.1 8.2.2.2 8.2.2.3 8.2.3 8.2.4 8.2.5 8.2.6 8.2.7	Applications of APPI and LPPI 267 Tiina J. Kauppila and Jack Syage Introduction 267 Atmospheric Pressure Photoionization 267 Atmospheric Pressure Photoionization Ion Source 267 General Principles of Atmospheric Pressure Photoionization 268 Ionization Mechanism in Positive Ion APPI 268 Effect of the Dopant 270 Ionization Mechanism in Negative Ion APPI 271 APPI in Liquid Chromatography Mass Spectrometry 272 APPI in Gas Chromatography Mass Spectrometry 274 APPI As an Interface for Capillary Electrophoresis Mass Spectrometry 277 APPI in Multimode Ion Sources 278 Ambient Mass Spectrometry Utilizing Photoionization 278
8.1 8.2 8.2.1 8.2.2 8.2.2.1 8.2.2.2 8.2.2.3 8.2.3 8.2.4 8.2.5 8.2.6 8.2.7 8.3 8.4 8.4.1	Applications of APPI and LPPI 267 Tiina J. Kauppila and Jack Syage Introduction 267 Atmospheric Pressure Photoionization 267 Atmospheric Pressure Photoionization Ion Source 267 General Principles of Atmospheric Pressure Photoionization 268 Ionization Mechanism in Positive Ion APPI 268 Effect of the Dopant 270 Ionization Mechanism in Negative Ion APPI 271 APPI in Liquid Chromatography Mass Spectrometry 272 APPI in Gas Chromatography Mass Spectrometry 274 APPI As an Interface for Capillary Electrophoresis Mass Spectrometry 277 APPI in Multimode Ion Sources 278 Ambient Mass Spectrometry Utilizing Photoionization 278 Low-Pressure Photoionization (LPPI) 279
8.1 8.2 8.2.1 8.2.2 8.2.2.1 8.2.2.2 8.2.2.3 8.2.3 8.2.4 8.2.5 8.2.6 8.2.7 8.3 8.4 8.4.1 8.4.2	Applications of APPI and LPPI 267 Tiina J. Kauppila and Jack Syage Introduction 267 Atmospheric Pressure Photoionization 267 Atmospheric Pressure Photoionization Ion Source 267 General Principles of Atmospheric Pressure Photoionization 268 Ionization Mechanism in Positive Ion APPI 268 Effect of the Dopant 270 Ionization Mechanism in Negative Ion APPI 271 APPI in Liquid Chromatography Mass Spectrometry 272 APPI in Gas Chromatography Mass Spectrometry 274 APPI As an Interface for Capillary Electrophoresis Mass Spectrometry 277 APPI in Multimode Ion Sources 278 Ambient Mass Spectrometry Utilizing Photoionization 278 Low-Pressure Photoionization (LPPI) 279 Applications of APPI and LPPI 281 Drugs, Pharmaceuticals, and Metabolites 281 Steroids 288
8.1 8.2 8.2.1 8.2.2 8.2.2.1 8.2.2.2 8.2.2.3 8.2.3 8.2.4 8.2.5 8.2.6 8.2.7 8.3 8.4 8.4.1 8.4.2 8.4.3	Applications of APPI and LPPI 267 Tiina J. Kauppila and Jack Syage Introduction 267 Atmospheric Pressure Photoionization 267 Atmospheric Pressure Photoionization Ion Source 267 General Principles of Atmospheric Pressure Photoionization 268 Ionization Mechanism in Positive Ion APPI 268 Effect of the Dopant 270 Ionization Mechanism in Negative Ion APPI 271 APPI in Liquid Chromatography Mass Spectrometry 272 APPI in Gas Chromatography Mass Spectrometry 274 APPI As an Interface for Capillary Electrophoresis Mass Spectrometry 277 APPI in Multimode Ion Sources 278 Ambient Mass Spectrometry Utilizing Photoionization 278 Low-Pressure Photoionization (LPPI) 279 Applications of APPI and LPPI 281 Drugs, Pharmaceuticals, and Metabolites 281 Steroids 288 Other Endogenic Compounds 288
8.1 8.2 8.2.1 8.2.2 8.2.2.1 8.2.2.2 8.2.2.3 8.2.3 8.2.4 8.2.5 8.2.6 8.2.7 8.3 8.4 8.4.1 8.4.2	Applications of APPI and LPPI 267 Tiina J. Kauppila and Jack Syage Introduction 267 Atmospheric Pressure Photoionization 267 Atmospheric Pressure Photoionization Ion Source 267 General Principles of Atmospheric Pressure Photoionization 268 Ionization Mechanism in Positive Ion APPI 268 Effect of the Dopant 270 Ionization Mechanism in Negative Ion APPI 271 APPI in Liquid Chromatography Mass Spectrometry 272 APPI in Gas Chromatography Mass Spectrometry 274 APPI As an Interface for Capillary Electrophoresis Mass Spectrometry 277 APPI in Multimode Ion Sources 278 Ambient Mass Spectrometry Utilizing Photoionization 278 Low-Pressure Photoionization (LPPI) 279 Applications of APPI and LPPI 281 Drugs, Pharmaceuticals, and Metabolites 281 Steroids 288

8.4.6	Oil Analysis 291
8.4.7	Food Analysis 291
8.5	Conclusions 292
	Acknowledgments 292
	References 292
9	Fundamentals of Laser Desorption Ionization 305
	Fabrizio Donnarumma, Kermit K. Murray, and Luke Hanley
9.1	Introduction 305
9.2	Experimental and Computational Parameters and Observables 306
9.3	General Mechanistic Considerations 307
9.4	Laser-Induced Thermal or Acoustic Desorption of Neutrals from Metal Surfaces 307
9.5	Molecular Resonantly Enhanced Desorption: UV-MALDI and IR-LA 309
9.5.1	MALDI with UV Lasers 310
9.5.2	Nanosecond to Picosecond IR Laser Ablation 313
9.6	Nanophotonic Desorption 314
9.7	Femtosecond Laser Ablation 315
9.8	Internal Energy Transferred by LDI and Supersonic Cooling 317
9.9	Conclusions 318
	Acknowledgments 319
	Disclosure Statement 319
	References 319
10	Applications of Laser Desorption Ionization and Laser
	Desorption/Ablation with Postionization 327
	Yeni P. Yung, Fabrizio Donnarumma, Kermit K. Murray, and Luke Hanley
10.1	Nature of Samples and Information to be Gained from Laser
	Desorption and Laser Ablation Mass Spectrometry 327
10.2	Laser Ablation and Laser Desorption Ionization MS for Elemental
	Analysis 328
10.3	Nonimaging MALDI-MS for Molecular Analysis 329
10.3.1	Qualitative and Quantitative Performance for Different Types of
	Analytes 329
10.3.2	Peptides, Proteins, Lipids, and Sugars 330
10.3.3	DNA and RNA 330
10.3.4	Polymers 331
10.4	MALDI-MS Imaging for Molecular Analyses 332
10.5	Example of Standard MALDI-MS vs. Imaging Mode: <i>Pseudomonas</i> aeruginosa 333
10.6	aeruginosa 333MALDI Alternatives: Matrix Free, Ambient, Nanostructure Induced,
10.0	and High Energy 335
10.7	Molecular LD/LA-MS Beyond Nanosecond UV Lasers 336
10.7	Laser, Electrospray, and Other Postionization of Plumes Formed by
10.0	LD/LA 337

Content	

10.8.1	LDPI-MS: Laser Desorption Postionization of Neutrals in Vacuum 337
10.8.2	Postionization Coupled to LD/LA at Elevated Pressures 340
10.9	Laser Ablation Sampling for Solid or Liquid Collection 341
10.9.1	Laser Ablation Sampling with Online MS Analysis 342
10.9.2	Laser Ablation Sampling with Off-line Analysis 343
10.7.2	Conclusions 344
10.10	
	Acknowledgments 345 Disclosure Statement 345
	References 345
	References 345
11	Laser Ionization in Single-Particle Mass Spectrometry 359
	Johannes Passig and Ralf Zimmermann
11.1	Relevance of Atmospheric Aerosols for Climate and Health – The
	Single-particle Perspective 359
11.2	Analysis of Individual Particles by Laser Ionization MS – Historical
	Development and Basic Principle 362
11.3	Ionization in Single-Particle Mass Spectrometry: Laser
	Desorption/Ionization (LDI) 365
11.3.1	Single-Particle LDI – The Physical Framework 366
11.3.2	Laser Light Sources for LDI 371
11.3.3	Chemical Quantification Approaches for LDI 372
11.4	Ionization in SPMS: Laser Photoionization of Previously Desorbed
	Species 373
11.5	Instrumental Realizations 381
11.5.1	Mass Analyzers 381
11.5.2	Aerosol Inlet 383
11.5.3	Particle Sizing 384
11.6	Data Evaluation 386
11.7	Applications 387
11.7.1	Ambient Aerosols in Urban and Densely Populated Areas 387
11.7.2	Ambient Aerosols in Rural and Marine Environments 388
11.7.3	Aircraft-Based Studies 389
11.7.4	In Situ Characterization of Cloud and Ice Condensation Nuclei 389
11.7.5	Focus on Organic Compounds 390
11.7.6	Bioaerosols 392
11.7.7	Combustion Aerosols 392
11.8	Commercial Laser Ionization Single-Particle Mass Spectrometry
11.0	Systems 393
	References 394
	MCICICIOCO J/I

Index 413

Preface

The goal of this book is to explain the fundamentals of photoionization (PI) and the associated applications of PI that are playing an increasingly important role in mass spectrometry (MS). The target audience of this book includes practicing scientists, including PhD and MSc students, whose primary interest is in the application of PI to elemental or molecular analysis by mass spectrometry. An overly simplistic analysis provides several motivations for the use of PI in mass spectrometry:

- 1. Enhance ion yields for specific important compounds of substance classes where other ionization strategies have proven insufficient,
- 2. Selectively ionize individual molecular structures or classes of molecules from mixtures,
- 3. Form ions from neutrals with reduced or controlled degree of fragmentation, and
- 4. Induce desorption or ablation of solids for sampling.

Photoionization comes in different versions and technological realizations, making it somewhat more complicated and thus less popular than standard ionization methods in mass spectrometry such as electrospray ionization and electron ionization. Nevertheless, one goal of this book is to demonstrate how these and other motivations drive the use of PI in MS-based analyses. The editors and authors hope that the readers will use this work as a series of building blocks for future advances in this promising area.

Actually, PI was central to the early development of mass spectrometry and single photon ionization (SPI) remains perhaps the best method for introducing a well-defined amount of internal energy into a molecular ion. Early work in SPI used vacuum ultraviolet (VUV) gas discharge lamps. However, the advent of lasers and the associated nonlinear optical methods made multiphoton ionization (MPI) possible, dramatically expanding PI as a fundamental strategy to probe molecular structure. The continuing improvement of laser technology has also created ongoing opportunities for MS-based applications of PI. For example, MPI via the excimer laser-pumped dye laser was deployed in many early fundamental studies, but was costly, difficult to use, and relatively unreliable. However, the development of smaller and rugged, field-deployable laser sources, such as compact excimer lasers, solid-state lasers as Nd:YAG lasers with integrated harmonic generation, and tunable solid-state lasers such as sealed,

Nd:YAG-pumped optical parametric oscillators (OPOs) or Ti:sapphire cavities rendered MPI sufficiently robust for more widespread MS applications.

This interplay between fundamental methods and instrumental considerations has driven the development of analytical applications of PI, so attention is paid here to both considerations. Photodissociation is only discussed here when it occurs in conjunction with PI, such as via the formation of fragment ions from neutral precursors during MPI or SPI. Thus, the burgeoning use of photodissociation of the precursor or molecular ions to form fragment ions for structural elucidation of the former is not discussed here. The fundamentals and mechanisms of low pressure, gas-phase molecular PI for mass spectrometry is covered in Chapters 1, 2, 5, and 7, while molecular atmospheric pressure PI is a topic in Chapter 8. Applications and experimental methods of low-pressure, gas-phase photoionization mass spectrometry (PIMS) are presented in Chapters 3, 4, and 7. Elemental analysis by PI is covered exclusively in Chapter 5. Processes and applications that include a laser desorption (LD) or direct laser desorption/ionization (LDI) of analytes from the condensed phase are covered in Chapters 9 and 10, while Chapter 11 focuses on the direct analysis of individual aerosol particles using LDI, LD, and PI.

In the following, the content of the book is briefly highlighted chapterwise.

The first chapter entitled FUNDAMENTALS and MECHANISMS of VACUUM PHOTOIONIZATION, is serving as an introduction to mechanistic issues common to PI of molecules, atoms, and clusters under vacuum. It provides a fundamental description of light and the interaction of light and matter in the form of photoabsorption on a quantum mechanical level. This includes an excursion in perturbation theory and the dipole approximation and leads to an elucidation of the photon absorption selection rules. Finally, the SPI process, as an absorption in a continuum, nonbound state, is discussed and the most important parameters for SPI, the SPI cross sections and ionization energies, are deducted.

Fundamental aspects of MPI of molecules in the absence of gas-phase collisions are covered in the following chapter, entitled FUNDAMENTALS and MECHANISMS of RESONANCE-ENHANCED MULTIPHOTON IONIZA-TION (REMPI) in VACUUM and APPLICATION of REMPI for MOLECULAR SPECTROSCOPY (Chapter 2). Here, the theoretical consideration of photoionization processes is extended to MPI processes of molecular species and MPI-based spectroscopy, while multiphoton ionization of atoms is covered in Chapter 6. Different MPI and REMPI processes are presented and a rate equation approach is used to deduct the influence of molecular physical properties on ionization efficiency. Special REMPI schemes are discussed, which can bypass unfavorable photophysical properties. In the following, MPI-induced fragmentation and dissociation processes are discussed. The application of REMPI for molecular spectroscopy with and without supersonic jet cooling is demonstrated in an exemplary manner via a detailed discussion of the REMPI wavelength spectrum of supersonic jet-cooled biphenylene and some other interesting aromatic molecules. REMPI wavelength spectroscopy, in particular with supersonic jet cooling, reveals the selectivity of the REMPI process that connects high-resolution ultraviolet (UV) spectroscopy to mass spectrometry. The selective ionization of isomeric and isobaric compounds, however, can be

extended to the differentiation of isotopomers and – by using a special REMPI technique with circular polarized laser light - even of enantiomers. Finally, in this chapter, REMPI-based photoelectron spectroscopic (PS) techniques such as zero kinetic energy photoelectron spectroscopic (ZEKE-PS) are introduced. The explanation of the fundamental aspects of SPI and REMPI leads to the analytical application of these two PI approaches.

In the beginning of Chapter 3, which is entitled "ANALYTICAL APPLICA-TIONS of SINGLE-PHOTON IONIZATION MASS SPECTROMETRY." a brief introduction into common VUV-light sources, is given. These can be distinguished as incoherent light sources ("lamp"-based technologies) or coherent light sources (lasers). Also, a brief introduction to the generation of synchrotron light in the VUV range is elaborated (for applications of synchrotron-based SPI, see Chapter 5). The general setup of SPI mass spectrometry systems with laser- and lamp-based sources is introduced. Depending on the used VUV wavelengths, SPI can be a very soft ionization method, enabling the detection of the molecular mass fingerprint of complex mixtures. This renders SPI-MS to an ideal approach for direct real time monitoring of complex gas and vapor mixtures. Different applications for online monitoring of combustion and pyrolysis processes are introduced, including online monitoring of gas phases from industrial processes, such as the coffee-roasting and/or the biomass pyrolysis process. Hyphenated instrumental analytical concepts, e.g. gas chromatography (GC) or thermal analysis (TA) coupled to SPI mass spectrometry, are presented and typical results are shown.

Chapter 4, "ANALYTICAL APPLICATION of RESONANCE-ENHANCED MULTIPHOTON IONIZATION MASS SPECTROMETRY (REMPI-MS)," gives, in a similar way as Chapter 3 for SPI, an overview of analytical applications of REMPI mass spectrometry. The preferential detection of aromatic analytes by the REMPI process with common laser is emphasized in Chapter 3. An overview on typical fixed-frequency laser lines (excimer lasers or frequency-multiplied, solid-state lasers) is provided along with typical wavelength ranges of tunable laser systems. In the following, several exemplary analytical concepts and applications using tunable and fixed-frequency lasers are presented. The tunable laser sources can be used to focus on specific analytes, which work particularly well with supersonic jet expansion inlet systems. For many applications, however, fixed-frequency wavelength laser and effusive, heated gas inlets can be applied for a useful and often very sensitive "overview" MS-profiling of many aromatic compounds. Exemplary process monitoring applications comprise detection of combustion by-products in flue gases of incineration plants or flavor and roast degree, indicating compounds in coffee-roasting off-gas. Hyphenated instruments connecting gas chromatography or a thermo-optical carbon analyzer (for aerosol loaded filters) to REMPI-MS devices are discussed. A direct inlet of liquid samples into REMPI mass spectrometry is possible via a membrane inlet or a direct liquid introduction into the ion source. Note that SPI and REMPI processes can be performed in the same MS system. Finally, REMPI under atmospheric conditions is discussed (atmospheric pressure laser ionization - APLI; see also Chapter 8 for SPI-based atmospheric pressure-based ionization).

The application of synchrotron VUV light for SPI-MS-based investigation of combustion and pyrolysis processes is laid out in Chapter 5, "PROBING CHEM-ISTRY AT VACUUM ULTRAVIOLET SYNCHROTRON LIGHT SOURCES." By direct molecular beam sampling from flames as well as from oxidation or pyrolysis reactors, molecules from the reaction zone can be directly introduced in the mass spectrometer without wall contact. This enables the analysis of stable molecules and intermediates from the reaction zones. The flow reactors and model flame apparatus is often compact enough to be brought to synchrotron light source facilities and can be used for kinetic investigations. Unlike classical VUV sources, the synchrotron light from appropriate beamlines (i.e. equipped with VUV monochromators) exhibit a wide tunability, high energy resolution, and a relatively high photon flux. The identification of individual compounds from isobaric mixture components is possible by photoionization efficiency (PIE) spectroscopy, i.e. the recording of the ion yield as a function of the VUV wavelength. Chapter 5 also presents, an overview on different synchrotron-based PIMS apparatus and analytical results for several reactors and applications.

REMPI of atoms is commonly referred to as "resonance ionization mass spectrometry (RIMS). The RIMS technology and applications are described in the Chapter 6, RESONANCE IONIZATION MASS SPECTROMETRY (RIMS): FUNDAMENTALS AND APPLICATIONS INCLUDING SECONDARY NEUTRAL MASS SPECTROMETRY. Unlike in molecules, atomic transitions are very narrow and thus very high ionization efficiencies can be achieved. Laser spectroscopic principles, atomic selection rules, and the principle setup of RIMS instruments are discussed. In many cases, two or more tunable lasers are required for high-resolution RIMS. This high effort, however, in many cases allows even an isotope-selective ionization and the suppression of nearly all interferences. Applications are focusing on the analyses of ultratraces of radioactive elements in the environment (e.g. plutonium fall out) or the characterization of very precious samples such as stardust grains.

MPI is often performed with nanosecond laser pulses, but shortening the pulses into the subpicosecond regime can fundamentally change the ionization process, as discussed in Chapter 7, "ULTRASHORT PULSE PHOTOIONIZA-TION for FEMTOSECOND LASER MASS SPECTROMETRY". The mechanisms of ultrashort pulse ionization, in particular nonresonant multiphoton ionization (NRMPI) and strong field ionization (SFI), are elucidated. One advantage of ultrashort pulse ionization is to overcome problems in REMPI ionization caused by the short lifetime of intermediated states (see also Chapter 2). Thus, for example, molecular ions of explosives, such as trinitrotoluene (TNT), which exhibit an unstable S₁ state due to fast predissociation (NO-cleavage from nitro groups), can be obtained by a fs-laser ionization process. In addition to gas-phase ionization, ultrashort pulse ionization is also beneficial for postionization of neutrals to enhance ion signal in secondary ion mass spectrometry (SIMS) or laser desorption (LD)-based mass spectrometry.

Mass spectrometry of samples at ambient pressure has become a major application, which is served by atmospheric pressure photoionization (APPI) using VUV for induction of the ionization process. Chapter 8, "PHOTOIONIZATION at ELEVATED or ATMOSPHERIC PRESSURE: APPLICATION of APPI and LPPI,"

is devoted to such ionization mechanisms at elevated pressures and their experimental implementation. Furthermore, some characteristic applications of APPI are shown. The higher pressures during APPI allow abundant gas-phase ion-molecule and molecule-molecule collisions that finally lead to energy and/or charge transfer in the APPI process. Therefore, very high sensitivities can be observed in APPI. However, although such secondary chemical ionization processes often are dominating the ionization process, APPI is commonly seen as a photoionization technology, although the term "photoinduced chemical ionization" may better describe the APPI process in many cases. In addition to SPI, the REMPI process can also be used to initiate ionization under atmospheric conditions (atmospheric pressure laser ionization, APLI, see Chapter 4).

Laser irradiation of condensed phase matter can also lead to PI as well as other energy transfer events that in turn lead to desorption and/or ablation that is widely used for sampling. Although this book is focusing on photoionization processes in vacuum or in the gas phase, laser desorption-based processes and applications in mass spectrometry are not be excluded. Chapter 9, "FUNDAMENTALS of LASER DESORPTION/IONIZATION," introduces the mechanisms of laser desorption/ionization (LDI) and matrix-assisted laser desorption/ionization (MALDI), while Chapter 10, "APPLICATIONS OF LASER DESORPTION IONIZATION AND LASER DESORPTION/ABLATION WITH POSTIONIZATION," introduces the corresponding applications. The MALDI approach for ionization of biopolymers (e.g. proteins or lipids), polymers, and other larger molecules is broadly applied, and numerous reviews and book chapters and whole books have already covered this topic. However, for completeness, the knowledge on the MALDI process is summarized in Chapter 9, although more focus is put on less common strategies such as fs-laser ablation. In the laser desorption applications discussed in Chapter 10, in addition to the molecular detection also, MALDI imaging applications are considered and a focus is put on the approaches using postionization of laser desorbed neutrals.

Finally, Chapter 11, "LASER IONIZATION in SINGLE-PARTICLE MASS SPECTROMETRY," elaborates on an online laser mass spectrometric single (aerosol)-particle measurement technique, which is based either on the LDI or on a laser desorption - laser postionization approach. After an introduction to the historical development of single-particle laser ionization MS systems, the LDI process is discussed in context of the particle analysis background. This includes the ionization mechanism, laser sources, and quantification aspects. After the discussion of approaches based on the laser postionization of molecules desorbed from individual particles, instrumental realizations and applications are presented and discussed.

Finally, we hope that the readers will enjoy and learn from our exposition of photoionization fundamentals as well as the versatility of the photoionization mass spectrometry methodology for cutting edge applications.

Ralf Zimmermann University of Rostock, Germany Luke Hanley University of Illinois, Chicago, USA

1

Fundamentals and Mechanisms of Vacuum Photoionization

Johannes Passig 1,2, Ralf Zimmermann 1,2, and Thomas Fennel³

1.1 Preface

Within the past decades, the progress of laser-based light sources have opened various new research directions in the area of light-matter interactions. The ionization of free molecules with the purpose of their detection and mass-based identification may appear as an easy task in this context. However, experience has shown that already the simplest approach, the fragment-free ionization with single photons of sufficient energy, remains technically challenging. Beyond practical issues and applications, advanced photoionization techniques are an important field of study in spectroscopy and fundamental research. As an example, resonance-enhanced multiphoton ionization (REMPI, see chapters 2 and 4 of this book) bridges the gap between mass spectrometry (MS) and molecular spectroscopy, offering two-dimensional selectivity both in mass and in structure. In general, the absorption of a single photon by a molecule can lead to its ionization if the photon energy $E = hv = \hbar\omega$ is equal to or larger than the ionization potential I_p , where $h=2\pi\hbar$ is the Planck constant, $v=c/\lambda$ is the photon frequency; λ is its wavelength, and c is the speed of light. It is worth to have a look on the typical energy- and timescales that constitute the framework of photoionization processes as illustrated in Figure 1.1. Electron motion and electronic transitions are much faster than atomic motion on molecular scales. This is the basis for important approximations in atom and molecular physics and spectroscopy. Current tabletop laser systems are available from infrared (IR) to ultraviolet (UV), with ultrashort pulses that allow to analyze molecular processes on their physical or natural timescale. Laser intensities for (multi-) photoionization MS span the range from the onset of REMPI ($\approx 10^6 \text{ W/cm}^2$) to the strong field regime ($> 10^{14} \text{ W/cm}^2$) and beyond for complex laser sources. Tuning the photon energy remains rather complicated both for lamp- and laser-based sources. However, the latter implicates further parameters as phase

¹ Universität Rostock, Institut für Chemie, Analytical Chemistry and Joint Mass Spectrometry Centre (JMSC), Dr.-Lorenz-Weg 2, D-18059 Rostock, Germany

²Helmholtz Zentrum München, German Research Center for Environmental Health GmbH, Research Unit Comprehensive Molecular Analytics (CMA) and Joint Mass Spectrometry Centre, Gmunder Str. 37, D-81379 München, Germany

³Institute of Physics, University of Rostock, Albert-Einstein-Straße 23, D-18059 Rostock, Germany

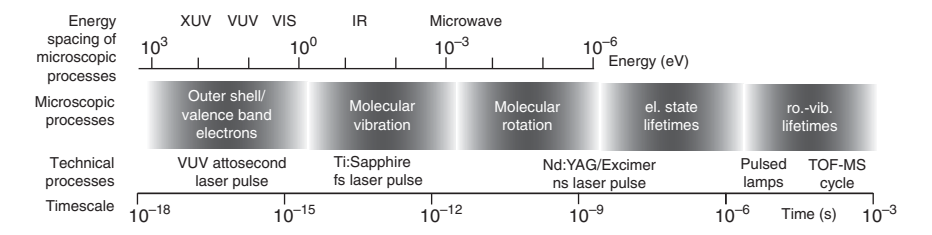


Figure 1.1 Typical energy- and timescales of processes related to photoionization.

or chirp, which are linked to the coherence of laser pulses and are likely to increase the selectivity in future applications.

When dealing with photoionization MS, natural questions about the underlying mechanisms of photoabsorption and photoionization arise at some point. A brief standard answer might be as follows: Assume two eigenstates of a molecular system with different electronic charge distributions. Upon excitation from the lower to the upper state and assuming a single active electron, the system corresponds to a quantum superposition of those two states and the electronic charge oscillates with an amplitude that reflects the transition dipole moment. Now, assume a light field acting on it. Thus, the electron "feels" an oscillating electric field from the light. If the frequencies, direction (polarization), and shape of charge distribution associated with a transition, match the light field and the molecule couple and the electron will be resonantly driven into the excited state while the light wave is damped. If the excited state is a continuum state, the electron is ejected.

This description provides a basic, phenomenological understanding, and some readers consider now to skip the following pages with complicated formulas. However, it is a problematic simplification, mixing different concepts and principles. The following section will provide an introductory survey on photoabsorption, being the physical basics of photoionization. The scope is not to treat the full complexity of optics and spectroscopy but to give an outline of some fundamental principles being useful for its conceptual understanding.

1.2 Light

The physics of classical light propagation, optics, and electromagnetism is based on the Maxwell equations, a set of partial differential equations that describe the behavior of the electric field $\mathbf{E}(\mathbf{r},t)$ and the magnetic field $\mathbf{B}(\mathbf{r},t)$ with respect to charges ρ and currents \mathbf{j} :

$$\nabla \cdot \mathbf{E}(\mathbf{r}, t) = \rho(\mathbf{r}, t) / \epsilon_0 \tag{1.1}$$

$$\nabla \cdot \mathbf{B}(\mathbf{r}, t) = 0 \tag{1.2}$$

$$\nabla \times \mathbf{E}(\mathbf{r}, t) = -\frac{\partial}{\partial t} \mathbf{B}(\mathbf{r}, t) \tag{1.3}$$

$$\nabla \times \mathbf{B}(\mathbf{r}, t) = \mu_0 \mathbf{j} + \mu_0 \epsilon_0 \frac{\partial}{\partial t} \mathbf{E}(\mathbf{r}, t)$$
 (1.4)

The divergence $\nabla \cdot \mathbf{F} = \frac{\partial F_x}{\partial x} + \frac{\partial F_y}{\partial y} + \frac{\partial F_z}{\partial z}$ of a vector field \mathbf{F} produces a scalar field, giving the quantity of F's source (outward flux) at each point. An expanding vector field (e.g. heated air) yields positive divergence values, whereas a contracting one (e.g., cooled air) yields negative values. The curl $\nabla \times \mathbf{F}$ yields a vector field that describes the infinitesimal rotation of F at each point, e.g. the circulation density of a flow.

Fundamental properties of light can be derived from this set of equations. Later, we will have to construct a Hamiltonian to describe photoabsorption. Because it represents the system total energy in quantum mechanics, it will be natural to use potentials rather than fields. In electrostatics, the field is related to the electrostatic potential through

$$\mathbf{E}(\mathbf{r}) = -\nabla \Phi(\mathbf{r}) \tag{1.5}$$

However, for a field that varies in time and in space, the electrodynamic potential must be expressed in terms of both the time-dependent scalar potential $\phi(\mathbf{r},t)$ and the vector potential $\mathbf{A}(\mathbf{r},t)$. According to Eq. (1.5), the fields $\mathbf{E}(\mathbf{r},t)$ and $\mathbf{B}(\mathbf{r},t)$ can be expressed as

$$\mathbf{E}(\mathbf{r},t) = -\nabla \phi(\mathbf{r},t) - \frac{\partial}{\partial t} \mathbf{A}(\mathbf{r},t)$$
(1.6)

$$\mathbf{B}(\mathbf{r},t) = \nabla \times \mathbf{A}(\mathbf{r},t) \tag{1.7}$$

This definition automatically fulfills Eqs. (1.2) and (1.3). Furthermore, it allows a transformation of the potentials into Coulomb gauge, where A is divergence-free ($\nabla \cdot \mathbf{A} = 0$), whereas the physical observables $\mathbf{E}(\mathbf{r}, t)$ and $\mathbf{B}(\mathbf{r}, t)$ remain unchanged (not shown here). In Coulomb gauge, the scalar potential is identical with the Coulomb potential, yielding $\phi = -\rho/\epsilon_0$ for Eq. (1.1). Furthermore, if charges and currents are absent, only Eq. (1.4) determines A (and thus **E** and **B**) in the following form of a wave equation:

$$\nabla^2 \mathbf{A}(\mathbf{r}, t) - \frac{1}{c^2} \frac{\partial^2}{\partial t^2} \mathbf{A}(\mathbf{r}, t) = 0 \text{ with } c^2 = \frac{1}{\sqrt{\mu_0 \epsilon_0}}$$
 (1.8)

Solutions are linearly polarized plane waves

$$\mathbf{A}(\mathbf{r},t) = \frac{1}{2}\tilde{A}\varepsilon e^{i(\mathbf{k}\cdot\mathbf{r}-\omega t)+\delta} + c.c. = \tilde{A}\varepsilon\cos(\mathbf{k}\cdot\mathbf{r}-\omega t+\delta)$$
 (1.9)

with amplitude \tilde{A} , polarization vector ε , imaginary unit i, wave vector k, angular frequency ω , and phase offset δ . Several primary properties of light can now be derived, such as the dispersion relation $\omega = ck$ when inserting the solution into Eq. (1.8) or the orthogonality of wave and polarization vectors $\mathbf{k} \cdot \mathbf{\varepsilon} = 0$ that directly results from the gauge condition $\nabla \cdot \mathbf{A} = 0$. The electric and magnetic fields follow as plane waves, mutually orthogonal also with the propagation direction due to the vector product $\mathbf{k} \times \varepsilon$

$$\mathbf{E}(\mathbf{r},t) = \tilde{E}\varepsilon \sin(\mathbf{k} \cdot \mathbf{r} - \omega t + \delta)$$
 (1.10)

$$\mathbf{B}(\mathbf{r},t) = \frac{\tilde{E}}{\omega}(\mathbf{k} \times \varepsilon) \sin(\mathbf{k} \cdot \mathbf{r} - \omega t + \delta)$$
 (1.11)

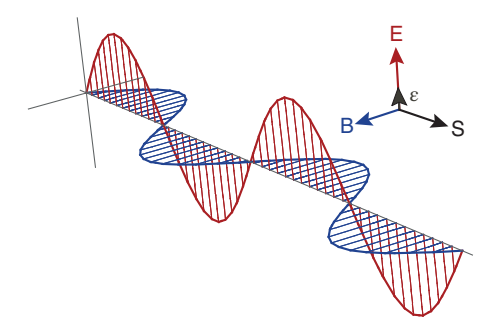


Figure 1.2 Illustration of a linearly polarized light wave as a solution of Eq. (1.8) with mutually orthogonal electric field **E**, magnetic field **B**, and propagation as well as energy transport in direction of the Poynting vector **S**. Polarization vector ε . Eq. (1.16).

with $\tilde{E} = -\omega \tilde{A}$. A key parameter for many applications is the light intensity, respectively the photon density. They follow from the (instantaneous) energy density of the electromagnetic field

$$u = \frac{1}{2} \left[\epsilon_0 |\mathbf{E}|^2 + \frac{1}{\mu_0} |\mathbf{B}|^2 \right] = \epsilon_0 \tilde{E}^2 \sin^2(\mathbf{k} \cdot \mathbf{r} - \omega t + \delta)$$
 (1.12)

The rapid oscillations can be averaged as $\langle \sin^2 \rangle = 1/2$, yielding the mean energy that can alternatively be expressed in terms of the photon density $n_{\rm ph} = dN_{\rm ph}/dV$

$$\langle u \rangle = \frac{1}{2} \epsilon_0 \tilde{E}^2 = n_{\rm ph} \hbar \omega \tag{1.13}$$

Energy transport by light propagation is characterized using the Poynting vector

$$\mathbf{S} = \frac{1}{\mu_0} \mathbf{E} \times \mathbf{B} = \epsilon_0 c \frac{\mathbf{k}}{k} \tilde{E}^2 \sin^2(\mathbf{k} \cdot \mathbf{r} - \omega t + \delta)$$
 (1.14)

The absolute value of its time-average $|\langle S \rangle|$ is the commonly used light intensity (unit W/m^2)

$$I = \frac{1}{2}\epsilon_0 c\tilde{E}^2 = c n_{\rm ph} \hbar \omega \tag{1.15}$$

Note that the intensity I is proportional to the square of the field (amplitude) \tilde{E}^2 . The photon flux φ (unit photons/(m² s)) can be expressed in terms of the intensity and photon energy or via the photon density $n_{\rm ph}$ and the speed of light c.

$$\varphi = \frac{I}{\hbar \omega} = n_{\rm ph} c \tag{1.16}$$

Next, the general cross section σ is a coefficient of proportionality between the rate W of an induced transition and the photon flux

$$W = \varphi \sigma(\omega) \tag{1.17}$$

with unit megabarn (1 Mb = 10^{-18} cm²).

1.3 **Photoabsorption**

In classical physics, light absorption is interpreted as damping of a periodic electric field by dipoles oscillating with opposite phase at the same frequency. This basic picture provides a descriptive explanation of optical properties and some fundamental interactions. However, a description of the photoionization of atoms and molecules is only possible in a quantum mechanical context. Upon light absorption, a system undergoes a transition from an initial state to a final state of higher energy with energy difference $\hbar\omega$. Because the charge distributions of the states differ, their coherent superposition results in an oscillating dipole that can couple to the light field under appropriate conditions.

1.3.1 **Transitions in First Order Perturbation Theory**

Some essential principles needed for the quantum mechanical description are the representation of (electronic) states by wavefunctions $\Psi(\mathbf{r},t)$ and physical observables by their corresponding operators.

In quantum mechanics, the state $|\psi\rangle$ of a system can be described by a complex wavefunction $\psi(\mathbf{r},t)$ in coordinate space representation. A physical observable is represented by a linear operator \hat{O} acting on the state producing a new vector $\hat{O}|\psi\rangle = |\psi^*\rangle$. If $|\psi\rangle$ is an eigenstate of an observable, the equation $\hat{O}|\psi\rangle = a \cdot |\psi\rangle$ yields the associated eigenvalues a_i corresponding to the value of the observable in that eigenstate. Eigenvalues a can be continuous (e.g. for the position operator $\hat{\mathbf{r}}$) or discrete as for the angular momentum operator and thus be expressed by quantum numbers.

The time evolution of a physical system is described by solutions of the time-dependent Schrödinger equation (TDSE) in its general form

$$i\hbar \frac{\partial}{\partial t} \Psi(\mathbf{r}, t) = \hat{H} \Psi(\mathbf{r}, t)$$
 (1.18)

where i is the imaginary unit, \hbar is the Planck constant, and \hat{H} is the Hamiltonian operator representing the system's total energy.

An analytical solution is only possible for very simple systems, such as the hydrogen atom. Already the presence of an external field or a second electron renders closed and analytical solutions impossible. Typically, several approximations allow for the treatment of a molecular system with minimum deficiency, depending on the framework of the scientific problem. Common approaches for atom-light interactions apply the single active electron approximation (SAE) that treats a single interacting electron in an effective potential (e.g. Hartree-Fock) resembling both the atomic core and the (mean) electron-electron interactions.

In general, photoionization can be understood as one of several possible secondary processes upon photoabsorption. For the weak field regime¹, which applies even beyond typical REMPI intensities of about 10⁷ W/cm², the description of photoabsorption is convenient via perturbation theory. Its basic concept is the partition of the Hamiltonian \hat{H} into the calculable Hamiltonian \hat{H}_0 of a simplified and known system (which may be artificial) and an additional Hamiltonian \hat{H}' representing the weak disturbance to the system that is quantified using approximate methods.

1.3.2 **Perturbation Theory**

For our basic considerations of photoabsorption via electronic states, we describe an atom by a single electron of charge q = e and mass $m_e = m$ in a Coulomb potential $V_C = -Ze^2/4\pi\epsilon_0 r$, which represents a stationary nucleus. The vector potential remains classical. Considering that in Coulomb gauge, the scalar potential equals V_C (see Section 1.2), the Hamiltonian of the electron splits into a stationary part of the undisturbed atom $\hat{H_0}$ and a time-dependent part $\hat{H}_{\mathrm{int}}(t)$ for the interaction with the light field. $\hat{H}_{\mathrm{int}}(t)$ can be derived from the classical Hamiltonian for a charged particle in a radiation field (not shown here)

$$\hat{H} = \underbrace{-\frac{\hbar^2}{2m} \nabla^2 + V_c}_{\hat{H}_0} - i\hbar \frac{e}{m} \mathbf{A} \cdot \nabla + \frac{q^2}{2m} A^2$$

$$(1.19)$$

For the first term \hat{H}_0 , the analogy to the corresponding classical total energy $E_{\rm kin}$ + $V=rac{p^2}{2m}+V$ is clearly visible, if the notation of the momentum operator $\hat{p}=-i\hbarrac{\partial}{\partial x}$ is considered.

For moderate field strengths ($I \ll 10^{15} \text{ W/cm}^2$), the last term is small compared to the cross term, which simplifies the interaction Hamiltonian H_{int} to

$$H_{\rm int} \approx -i\hbar \frac{e}{m} \mathbf{A} \cdot \mathbf{\nabla} \tag{1.20}$$

According to perturbation theory, the wavefunction $\Psi(\mathbf{r},t)$ can be expressed as a linear combination of unperturbated eigenstates $\Psi(\mathbf{r})$ of the stationary Schrödinger equation (time-independent Hamiltonian) $H_0\Psi_i(\mathbf{r}) = E_i\Psi_i(\mathbf{r})$ with the time-dependent coefficients $c_i(t)$

$$\Psi(\mathbf{r},t) = \sum_{j} c_{j}(t)\Psi_{j}(\mathbf{r})e^{-iE_{j}t/\hbar}$$
(1.21)

¹ The term "weak disturbance" indicates an important limitation for laser-based photoionization: The external laser field, treated as perturbation, has to be small against the inner atomic forces. Thus, laser intensities exceeding 10¹² W/cm² and molecular interactions induced thereby are often referred to as "nonperturbative" (Baumert and Gerber 1997), while typical intensities for single-photon ionization (SPI) and REMPI applications are below 10⁸ W/cm².

Inserting in the TDSE (Eq. (1.18)) yields

$$\sum_{j} (i\hbar \frac{d}{dt} c_j(t) + E_j) e^{-iE_j t/\hbar} |\Psi_j\rangle = \sum_{k} (E_k + H_{\text{int}}(t)) c_k(t) e^{-iE_k t/\hbar} |\Psi_k\rangle \qquad (1.22)$$

The "ket" vector $|\Psi\rangle$ represents the state that is associated with the wavefunction $\Psi(r,t)$. With the corresponding "bra" vector $\langle \Psi |$, that corresponds to the complex conjugated wavefunction $\Psi^*(r,t)$ in coordinate space, and with the inner product $\langle \Psi | \Psi \rangle = \int \Psi^* \Psi dr$ and the operator H acting on $|\Psi\rangle$, we can express the expectation value of the observable (here energy) represented by operator H in the state $|\Psi\rangle$ by $\langle\Psi|H|\Psi\rangle$.

Considering the orthogonality of the eigenstates, the result is a set of coupled equations for the time evolution of coefficients $c_i(t)$ with the transition frequency $\omega_{ik} = (E_i - E_k)/\hbar$:

$$\frac{d}{dt}c_{j}(t) = \frac{1}{i\hbar} \sum_{k} \underbrace{\langle \Psi_{j} | H_{\text{int}}(t) | \Psi_{k} \rangle}_{H_{\text{int}}^{(k)}(t)} c_{k}(t) e^{i\omega_{jk}t}$$
(1.23)

Assuming a two-level system with initial state $|\Psi_a\rangle$ and the interaction Hamiltonian (1.20), the coefficient $c_h(t)$ for the state $|\Psi_h\rangle$ can be expressed in the following form.

$$c_b(t) = \frac{1}{i\hbar} \int_0^t H_{\text{int}}^{ba}(t') e^{i\omega_{ba}t'} dt' = -\frac{e}{m} \int_0^t \langle \Psi_b | \mathbf{A} \cdot \nabla | \Psi_a \rangle e^{i\omega_{ba}t'} dt' \qquad (1.24)$$

Applying the vector potential **A** for the electromagnetic field representing the classic description of light (Section 1.2)

$$\mathbf{A}(\mathbf{r},t) = \tilde{A}\varepsilon \cos(\mathbf{k}\mathbf{r} - \omega t + \delta) = \frac{1}{2}\tilde{A}\varepsilon[e^{i(\mathbf{k}\mathbf{r} - \omega t + \delta)} + e^{-i(\mathbf{k}\mathbf{r} - \omega t + \delta)}]$$
(1.25)

yields the time-dependent amplitude of state $|\Psi_h\rangle$ in first-order perturbation theory

$$\begin{split} c_b(t) &= -\frac{e}{2m} \tilde{A} [e^{i\delta} \langle \Psi_b | e^{i\mathbf{k}\mathbf{r}} \varepsilon \cdot \nabla | \Psi_a \rangle \int_0^t e^{i(\omega_{ba} - \omega)t'} dt' \\ &+ e^{-i\delta} \langle \Psi_b | e^{-i\mathbf{k}\mathbf{r}} \varepsilon \cdot \nabla | \Psi_a \rangle \int_0^t e^{i(\omega_{ba} + \omega)t'} dt'] \end{split} \tag{1.26}$$

The first integral describes the absorption of a photon. Because the complex *e*-function is periodic with mean value zero for $\omega_{ba} \neq \omega$, it contributes only for $\omega_{ba} = \omega \Rightarrow E_b = E_a + \hbar \omega$ while the second integral corresponds to the photon emission if $\omega_{ba} = -\omega \Rightarrow E_b = E_a - \hbar\omega$.

Absorption

The matrix element associated with the perturbation $M_{ba}(\omega) = \langle \Psi_b | e^{i\mathbf{k}\mathbf{r}} \varepsilon \cdot \nabla | \Psi_a \rangle$ in Eq. (1.26) connects the initial state with the final state and thus determines the system interaction strength with the light. Before its further evaluation, we

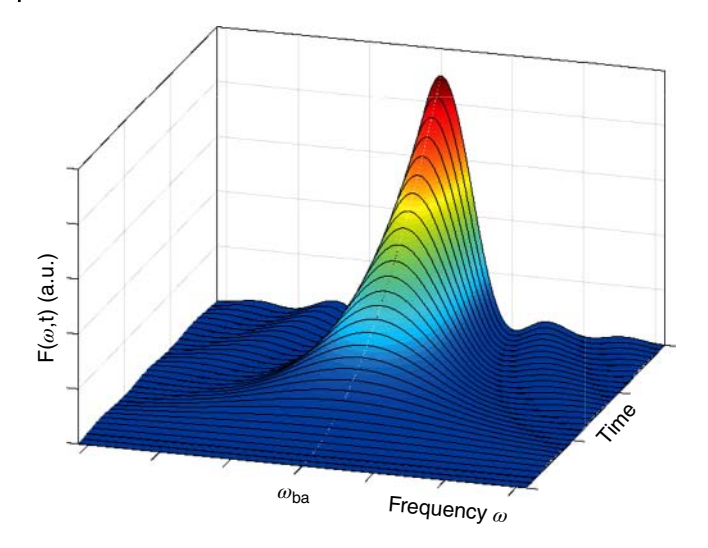


Figure 1.3 Behavior of the function $F(\omega,t)$ (Eq. (1.28)) that determines the time evolution of the transition when the field and the system are in resonance. If the light frequency ω equals the transition frequency ω_{ba} of the states $|\Psi_a\rangle$ and $|\Psi_b\rangle$, the function peaks increasingly and transforms into the δ-function in the long-time limit.

derive corresponding transition rates and cross sections. During absorption, the occupation probability $c_b(t)$ of the state $|\Psi_b\rangle$ increases with time, which can be expressed through integration of the first term in Eq. (1.26)

$$|c_b(t)|^2 = \left| -\frac{e}{2mi} \tilde{A} e^{i\delta} M_{ba}(\omega) \frac{e^{i(\omega_{ba} - \omega)t} - 1}{\omega_{ba} - \omega} \right|^2 = \frac{1}{2} \frac{e^2}{m^2} \tilde{A}^2 |M_{ab}(\omega)|^2 F(t, \tilde{\omega})$$

$$(1.27)$$

with

$$F(t,\tilde{\omega}) = \frac{1 - \cos(\tilde{\omega}t)}{\tilde{\omega}^2} \tag{1.28}$$

and the frequency offset $\tilde{\omega} = \omega - \omega_{ba}$. As illustrated in Figure 1.3, the transition probability increases sharply with time according to function (1.28) when the external field and the system are in *resonance*, hence $\omega = \omega_{ba}$.

Equations (1.27) and (1.28) describe the evolution of the occupation probability of state $|\Psi_b\rangle$ with time and thus characterize the rate with which transitions appears. During excitation, the states $|\Psi_a\rangle$ and $|\Psi_b\rangle$ form a coherent superposition and the associated dipole oscillates with the transition frequency.

For timescales longer than a cycle $(t \gg 2\pi/|\omega_{ba}|)$, Eq. (1.28) changes to a delta function $F(t,\tilde{\omega}) \Rightarrow \pi t \delta(\omega - \omega_{ba})$ (note: $\delta(\tilde{\omega}) \to \infty$ for $\tilde{\omega} \to 0$). Furthermore, we express the amplitude \tilde{A} of the vector potential by the light intensity I (compare Eq. (1.15)).

$$\tilde{A}^2 = \frac{2I}{\epsilon_0 c \omega^2} \tag{1.29}$$

and find the frequency-dependent absorption rate

$$W_{ba}(\omega) = \frac{\pi e^2}{\epsilon_0 \text{cm}^2} \frac{I}{\omega^2} |M_{ba}(\omega)|^2 \delta(\omega - \omega_{ba})$$
 (1.30)

So far, we assumed perfectly monochromatic light corresponding to an infinite plane wave. However, the intensity of realistic light has components covering at least a narrow band over a frequency range $I(\omega) = dI/d\omega$; thus, the total absorption rate has to be integrated over the entire spectrum

$$W_{ba} = \int W_{ba}(\omega)I(\omega)d\omega \tag{1.31}$$

In the long-time limit, only the value at ω_{ba} contributes to W_{ba} by nature of the delta function

$$W_{ba} = \frac{\pi e^2}{\epsilon_0 \text{cm}^2} \frac{I(\omega_{ba})}{\omega_{ba}^2} |M_{ba}(\omega_{ba})|^2$$
(1.32)

To express the associated cross section, we use Eq. (1.17)

$$\hbar\omega_{ba}W_{ba} = I(\omega_{ba})\sigma_{ba} \tag{1.33}$$

which yields the absorption cross section for the spectral intensity associated with the considered transition. Note that the unit of the cross section is therefore area times frequency.

$$\sigma_{ba} = \frac{\pi\hbar}{\epsilon_0 c} \frac{e^2}{m^2} \frac{1}{\omega_{ba}} |M_{ba}(\omega_{ba})|^2 \tag{1.34}$$

Of note, the integration (1.31) assumes a sum of incoherent spectral components. The treatment of absorption from coherent and ultrashort laser pulses has to consider the explicit pulse waveform.

Molecules typically have numerous states in a small energy interval that contributes to the absorption. Hence, the transition probability into this band is the sum of all transition probabilities matching the frequency of the incident light. The number of states in an energy range between E_b and $E_b + dE$ can be expressed as $\rho(E_b)dE$, where $\rho(E_b)$ is called the density of states. Assuming that the matrix elements for transitions into such a band of states are comparable, Fermi's golden rule can be derived via spectral integration of the transition rates (not shown).

$$W_{ba} = \frac{2\pi}{\hbar} \rho(E_b) |M_{ba}|^2 \tag{1.35}$$

Thus, to calculate the transition rate into a band, multiply the square of the matrix element by the density of states of the involved bands.

1.3.4 **Dipole Approximation**

So far, the matrix elements are dependent on the wavelength and direction of the light wave (photon) via the $e^{i\mathbf{k}\mathbf{r}}$ term. For interactions with visible, (V)UV, and IR (but not X-ray) radiation, the wavelength is much larger than the atomic length scale; hence, the system "feels" an oscillating dipole field. As a consequence, the wave vector dependence of the vector potential can be neglected, according to $e^{i\mathbf{k}\mathbf{r}} \approx 1$ for $\lambda \to \infty$; $\mathbf{k} \to 0$. In this so-called dipole approximation, the vector potential $A(\mathbf{r}, t) \to A(t)$ describing the light field becomes spatially homogenous and, as a consequence, the magnetic field $\mathbf{B} = \nabla \times \mathbf{A}$ vanishes. Descriptively, the electron velocity \mathbf{v}_e is low enough to neglect both the magnetic Lorentz force $e(\mathbf{v}_e \times \mathbf{B})$ and the relativistic effects that arise if the electron is driven at very high intensities (> 10¹⁶ W/cm²), predominantly for long wavelengths. The matrix elements ${\cal M}_{ha}^D$ can now expressed by the dipole matrix element in the so-called length form via the transition dipole moment $\mathbf{D}_{ba} = -e\mathbf{r}_{ba}$ containing spatial coordinates $(\hat{x}, \hat{y}, \hat{z})$ of the position operator **r**

$$M_{ba}^{D} = \frac{m\omega_{ba}}{\hbar e} \varepsilon \cdot (-e\langle \Psi_{b} | \mathbf{r} | \Psi_{a} \rangle) = \frac{m\omega_{ba}}{\hbar e} \varepsilon \cdot \mathbf{D}_{ba}$$
(1.36)

Thus, the matrix element of the interaction Hamiltonian, representing the expectation value of its energy spectrum, is now related to the much more descriptive dipole matrix element \mathbf{D}_{ha} , which represents the charge distribution within the wavefunction.

The dipole matrix element \mathbf{D}_{ba} (and also M_{ba}) determines the interaction strength between light and the atom or molecule. Its scalar part describes the change of charge distribution during transition from $|\Psi_a\rangle$ to $|\Psi_b\rangle$ that determines the transition probability. The vector part demands projection of the light field onto the dipole moment, i.e. it defines the required light polarization.

The corresponding absorption rate can be derived to

$$W_{ba}^{D} = \frac{\pi}{3\epsilon_{0}c\hbar^{2}}I(\omega_{ba})|\mathbf{D}_{ba}|^{2} = \frac{\pi e^{2}}{3\epsilon_{0}c\hbar^{2}}I(\omega_{ba})|\mathbf{r}_{ba}|^{2}$$
(1.37)

If the dipole matrix element is zero, the transition is so-called dipole-forbidden. However, such transitions are often observed because they may be allowed as (weaker) magnetic dipole or electric quadrupole transitions. Commonly used in spectroscopy to describe the absorption strength is the dimensionless oscillator strength f_{ii} of a transition between states i and j

$$f_{ij} = \frac{2m_e \omega_{ij}}{3\hbar} |\mathbf{r}_{ij}|^2 \tag{1.38}$$

Oscillator strength values are between 0 and 1. Typical values are shown in Table 1.2.

An interesting application of transition rates is related to the famous Einstein coefficients. Therefore, the Boltzmann distribution is applied to the level population of an ensemble of atoms in equilibrium and the Planck distribution to the photon field. An interesting finding in the context of VUV sources is that spontaneous emission increases relative to stimulated emission as the cube of light frequency. Hence, population inversion, which is a basis of laser sources, is difficult to generate and maintain in highly excited systems. Instead of cooperating in a stimulated emission process, the excited populations randomly loose energy via spontaneous emission.

Selection Rules 1.3.5

To calculate absorption rates, the corresponding matrix elements have to be evaluated by spatial integration over the corresponding wave functions $\langle \Psi_b | \mathbf{r} | \Psi_a \rangle = \int \Psi_b \mathbf{r} \Psi_a d\mathbf{r}$ in Eq. (1.36). If the integral vanishes, a transition does not occur (with the exception of higher order transitions), which is called dipole-forbidden. In particular, this is the case if the function $\Psi_b \mathbf{r} \Psi_a$ is antisymmetric, and thus, its integral over space yields zero. This can often be determined by analysis of the wavefunction symmetry without explicit calculation of the integral. For example, dipole transitions (e.g. $|s\rangle \rightarrow |s\rangle$) are not allowed for the hydrogen atom. The symmetry behavior is reflected by the parity selection rule (ref. third column in Table 1.1). Using quantum numbers to term the states, further selection rules for dipole transitions can be derived by evaluation of zero and nonzero matrix elements, as $\Delta l = \pm 1$ and $\Delta m = 0, \pm 1$, where l is the angular momentum quantum number and m is the magnetic quantum number in a one-electron system. Descriptively, these rules reflect conservation of angular momentum because the spin of the absorbed photon contributes to the system's angular momentum L. The z-component of L is associated with the electrons' magnetic moment, which couples to the photon spin, thus yielding $\Delta m = 0$ in the case of linear polarization and $\Delta m = \pm 1$ for circularly polarized light. For multielectron systems, the total angular and orbital momentum as well as the total spin is evaluated, and coupling schemes of angular momentum sources are considered. In realistic systems, especially molecules, several dipole-forbidden transitions can nevertheless be observed. For example, the dipole-forbidden transitions may be allowed as multipole transitions. Typically, the rate drops down by three orders of magnitude from one multipole to the next, see Table 1.2.

1.3.6 Electronic Line Width and Lifetime

So far, we assumed that the states have sharp eigen energies and can be described via time-dependent wavefunctions of the form $\psi e^{-iEt/\hbar}$ (ref. Figure 1.4a,d). Suppose a state that is exponentially decaying in amplitude as the system changes to another state (Figure 1.4b). The decaying function corresponds

Table 1.1 Dipole selection rules for electronic transitions in a Hydrogen-like atom. J = L + S is the total angular momentum, L is the total orbital momentum quantum number, S is the total spin quantum number, M_i is the total magnetic quantum number, and π is the parity.

	Rigorous			LS coupling	Intermediate coupling
$\Delta J = 0, \pm 1$	$\Delta M_J = 0, \pm 1$	$\pi_b = -\pi_a$	$^{a)}$ $\Delta l = \pm 1$	^{b)} if $\Delta S = 0$:	c) if $\Delta S = \pm 1$:
$(J=0 \Leftrightarrow 0)$				$\Delta L = 0, \pm 1, (L = 0 \Leftrightarrow 0)$	$\Delta L=0,\pm 1,\pm 2$

a) Rigorous for one-electron systems.

b) Small atoms with low LS-coupling.

Heavier atoms with transitions between several multiplet states.

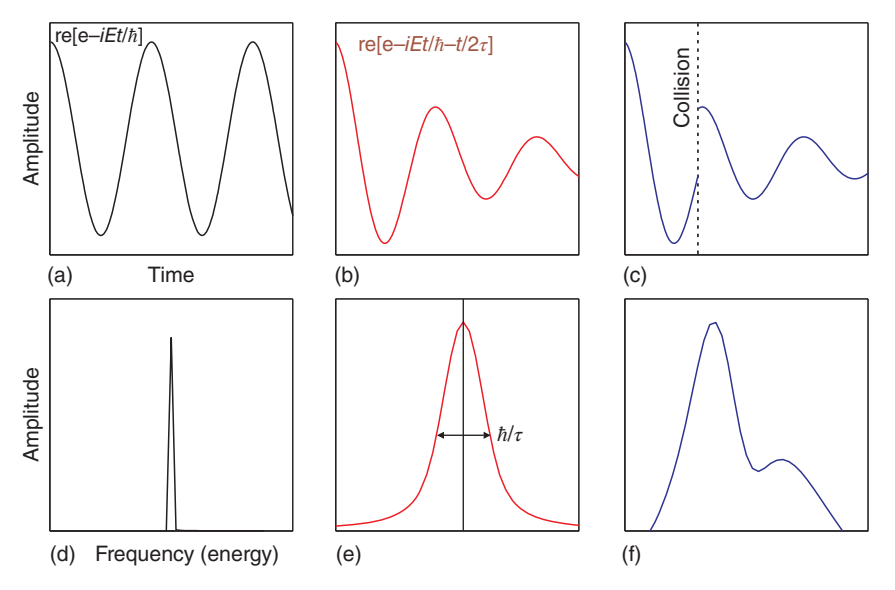


Figure 1.4 Schematic wavefunctions (top) and their spectra (bottom). (a, d) Stationary state. (b, e) Decaying state and resulting Lorentzian line profile. (c, f) Collision-induced phase distortion and its resulting spectrum (fast Fourier transformed).

to a superposition of oscillations whose frequencies can be Fourier analyzed according to

$$e^{-iEt/\hbar - t/\tau} = \int g(E')e^{-iE't/\hbar}dE' \text{ with } g(E') = \frac{1}{\pi} \frac{(\hbar/\tau)}{(E - E')^2 + (\hbar/\tau)^2}$$
 (1.39)

where τ is the time constant of the decay. Therefore, the decaying dipole oscillation is associated with a finite energy range. The width at half height of the Lorentzian function g(E') is \hbar/τ and called *natural line width* (Figure 1.4e). Considering that the state to which the transition appears may also have a finite lifetime τ_b , the line width is given by

$$\delta E = \hbar \left(\frac{1}{\tau_b} + \frac{1}{\tau_a} \right) \tag{1.40}$$

Hence, the shorter the state lifetime, the less precise its energy and vice versa. This concept is particularly important for REMPI (see Chapter 2), where ionization rates depend on the energy match between the photon and possible intermediate states as well as the photon density. It further gives rise to the concept of virtual states of uncertain energy, which may be employed at high photon densities.

Measured line widths are typically much larger, which can be attributed to the other origins of broadening. First, collisions with other atoms may lead to (radiative or nonradiative) transitions and randomize the phase of emitted radiation (ref. Fig. 1.4c,f). Both reduces the effective lifetime of the state and leads to the (pressure-dependent) *collision broadening* of the Lorentzian line profile. Secondary, the relative motion of atoms results in frequency shift. Thus, the so-called *Doppler broadening* increases with temperature and decreases